RKKY quadratic and biquadratic spin-spin interactions in twisted bilayer graphene

Oriekhov, D. O.; Osterholt, T. T.; Duine, R. A.; Gusynin, V. P.

DOI
10.1103/wkp4-2n5b

Publication date
2025

Document Version
Final published version

Published in
Physical Review B

RKKY quadratic and biquadratic spin-spin interactions in twisted bilayer graphene

D. O. Oriekhov [1], T. T. Osterholt [2], R. A. Duine [2,3] and V. P. Gusynin [4]
[1]*Kavli Institute of Nanoscience, Delft University of Technology, 2628 CJ Delft, The Netherlands*
[2]*Institute for Theoretical Physics, Utrecht University, Princetonplein 5, 3584CC Utrecht, The Netherlands*
[3]*Department of Applied Physics, Eindhoven University of Technology, P.O. Box 513, 5600 MB Eindhoven, The Netherlands*
[4]*Bogolyubov Institute for Theoretical Physics, Kyiv 03143, Ukraine*

(Received 6 February 2025; revised 5 June 2025; accepted 8 July 2025; published 24 July 2025)

We study the competition between the Ruderman-Kittel-Kasuya-Yosida (RKKY) quadratic and biquadratic spin-spin interactions of two magnetic impurities in twisted bilayer graphene away from the magic angle. We apply the Bistritzer-MacDonald model of two graphene layers twisted with respect to each other by a small angle. By reducing the model to the Dirac-type one with modified Fermi velocity, we derive expressions for the RKKY quadratic and biquadratic spin interactions using perturbation theory for the free energy. The biquadratic interaction is suppressed by a larger power of the interaction constant and decreases faster with the distance between impurities compared to the quadratic one. Nevertheless, due to the different period of the oscillations with the impurity separation distance, chemical potential, twist angle, and temperature, it is possible to fine-tune the system to the regime of dominating biquadratic interaction. The existence of such a fine-tuned regime might provide a promising opportunity to observe nonconventional spin ordering.

DOI: 10.1103/wkp4-2n5b

I. INTRODUCTION

The study of exchange spin-spin interactions started from the pioneering work of Heisenberg on ferromagnetism [1]. One of the key questions arising for all spin-spin interaction problems is the role of the surrounding medium. A milestone in studies of the foundational principles of magnets was reached with the discovery of the Ruderman-Kittel-Kasuya-Yosida (RKKY) interaction [2–4], which describes the exchange interaction between two magnetic impurities induced by the conduction electrons of the medium. This usually appears as a leading-order contribution from perturbation theory in the coupling constant between spin impurities and valence electrons of the underlying material. Integrating out the electronic degrees of freedom, one obtains the contribution of the exchange interaction to the total free energy of the system. However, as pointed out in Ref. [5], little is known about the next higher-order spin-spin interactions coming from the next terms in perturbation theory. The simplest non-Heisenberg coupling term of this kind that should be taken into account represents a biquadratic interaction: For two impurities with spins $\boldsymbol{S}_1$ and $\boldsymbol{S}_2$ it has the form $(\boldsymbol{S}_1\boldsymbol{S}_2)^2$ for isotropic systems, whereas the standard RKKY term is $\boldsymbol{S}_1\boldsymbol{S}_2$.

The model with biquadratic interaction was applied in Ref. [5] to describe magnetic phenomena in layered magnets such as CrI_3 and $CrBr_3$. A number of candidate materials in which biquadratic spin couplings play a key role, such as NiX_2 (X = Cl, Br, and I) [6] and iron-based superconductors [7], have been studied. Theoretical studies of effective bilinear-biquadratic models of magnets with both RKKY quadratic and biquadratic interactions found that unconventional magnetic order parameters can be formed: quadrupole [8,9], spiral, stripe, and tetrahedral orders [7,10]. In addition, a large biquadratic interaction constant is expected to stabilize the ferromagnetic state in NiX_2 (X = Cl, Br, and I) [6].

Usually, biquadratic spin-spin interactions are added to phenomenological spin Hamiltonians to describe the stability and competition of different phases of the system. Very rarely are such interactions derived from more microscopic theories. We will consider such a derivation in this article, where we use the reduced low-energy Hamiltonian of the Bistritzer-MacDonald model [11] for twisted bilayer graphene as a microscopic Hamiltonian. The model system is presented in Fig. 1. The idea of twisting graphene layers to exploit an additional twist angle degree of freedom to vary interlayer electronic hopping terms was first proposed in Ref. [12] and tested experimentally in Ref. [13]. The famous seminal paper by Bistritzer and MacDonald [11] found that at a specific ("magic") angle a flat band is formed after complete flattening of the Dirac cone. Later, this prediction was confirmed in a number of experiments [14,15], leading to the first observation of superconductivity in bilayer graphene without heavy doping.

In the present paper we focus on twist angles that are away from the first magic angle, where the Dirac cone remains. The corresponding model used in this study is obtained from

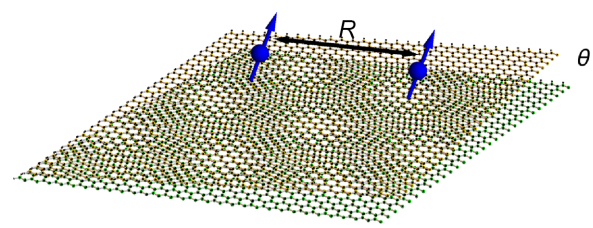

FIG. 1. Schematic representation of the system considered in this paper: Two impurities are placed on top of twisted bilayer graphene with layer rotation angle θ. It is assumed that impurities are placed near individual atoms. The distance between impurities equals R.

the Bistritzer-MacDonald model. It reduces to an effective two-component Dirac Hamiltonian with modified Fermi velocity depending on the rotation angle [16,17]. This allows for complete analytic treatment of the RKKY interaction for all parameters [18] and at zero temperature for the biquadratic interaction. The main finding of this paper is that the biquadratic interaction has a different oscillation period with distance and doping compared to the RKKY second-order term at zero temperature. This implies a specific selection of a twist angle and impurity location where the spin ordering will be predominantly determined by the biquadratic interaction.

This paper is organized as follows: We start by introducing the effective model of twisted bilayer graphene in Sec. II. Next, using the free energy expression, we derive the contribution of the biquadratic interaction in terms of the Green's functions of the free electron in Sec. III and obtain analytic expressions for interaction integrals in Sec. III A. Next, we present results for the zero-temperature case in Sec. IV and discuss the possibility of detecting biquadratic interaction at certain fine-tuned values of the twist angle for given impurity positions. In Sec. V we analyze the role of finite temperature using numerically evaluated expressions for interaction integrals. We present conclusions in Sec. VI. Finally, as an example, Appendix B contains the calculation of the interaction integral to the second order of perturbation theory.

II. THE EFFECTIVE MODEL OF TWISTED BILAYER GRAPHENE

We start with the Bistritzer-MacDonald (BM) model [11]. It is obtained in the vicinity of a single K point by taking into account the fast decay of the interlayer hopping parameter with distance. The BM model contains in total eight spin-degenerate bands and reduces to the following effective linearized model for the two lowest-energy bands [11,16,17] with an effective Hamiltonian:

$$H_{\text{eff}}(\mathbf{k}) = \hbar v_F^*(\tau_x k_x + \xi\tau_y k_y),\ v_F^* = \left(\frac{1-3\alpha^2}{1+6\alpha^2}\right)v_F, \quad (1)$$

where v_F^* is the effective Fermi velocity, Pauli matrices τ_x and τ_y act on the layer degree of freedom in the spinor wave function, and ξ is the valley index. The parameters in v_F^* are defined through the twist angle θ and parameters of monolayer graphene as

$$\alpha = w/\hbar v_F k_\theta, \quad k_\theta = 8\pi\sin(\theta/2)/3a_0. \quad (2)$$

The numerical values used throughout the paper are the Fermi velocity of monolayer graphene $v_F = \sqrt{3}ta_0/2\hbar = 9.3\times10^7$ cm/s, lattice constant $a_0 = 0.246$ nm, and the magnitude of the interlayer hopping parameter $w = 110$ meV. The approximation used to obtain Eq. (1) imposes particle-hole symmetry. For magic values of the angle, the effective Fermi velocity vanishes, and the next order of the expansion in a wave vector should be taken into account. This results in the appearance of Van Hove singularities close to charge neutrality point [11,19,20], for which the calculation of spin-spin interactions in the perturbation theory would present a challenge due to the divergent density of states. Thus, the calculations below always assume a finite value of the effective Fermi velocity. The model (1) should work decently well in the range of twist angles between $\theta \approx 0.8^\circ$ and $\theta = 10^\circ$, where the lower bound estimated from the middle of the interval between first and second magic angles is at 1.05° and 0.5°, respectively; the upper bound was numerically estimated from the applicability of Bloch's functions in Ref. [11]. The energy range of the applicability of the full BM model and of the linearized two-band model is estimated to be up to 1 eV from the charge-neutrality point [11,16,17].

The retarded Green's function of the model (1) is given by

$$G_0^R(\omega,\mathbf{k},\xi) = \frac{\omega + \hbar v_F^*(\tau_x k_x + \xi\tau_y k_y)}{(\omega+i\varepsilon)^2 - (\hbar v_F^*)^2\mathbf{k}^2}. \quad (3)$$

Using the results from monolayer graphene with reduced Fermi velocity, the real space version of the Green's function for a given valley index ξ takes the form

$$G_0^R(\mathbf{r},\omega,\xi) = \frac{\omega}{4(\hbar v_F^*)^2} \times \begin{pmatrix} -iH_0^{(1)}(z)\xi & e^{-i\xi\varphi}H_1^{(1)}(z) \\ \xi e^{i\xi\varphi}H_1^{(1)}(z) & -iH_0^{(1)}(z) \end{pmatrix}, \quad z = \frac{|\mathbf{r}|(\omega+i\varepsilon)}{\hbar v_F^*}. \quad (4)$$

Here $H_i^{(1)}(z)$ is the Hankel function of the first kind, and φ is the polar angle measured from the x axis.

In the following sections we perform the calculation for only a single valley ξ to extract the behavior of RKKY quadratic and biquadratic interactions that is sensitive to Fermi velocity changes due to the twist angle. Later, we discuss the effects of taking into account two valleys in the moiré Brillouin zone.

III. DERIVATION OF THE RKKY QUADRATIC AND BIQUADRATIC INTERACTIONS

For the purpose of deriving a general expression for the biquadratic interaction from perturbation theory, we start with the free energy expressed through the partition function as $F = -T\ln Z$:

$$Z = Z_0^{-1}\int \mathcal{D}\psi\mathcal{D}\psi^\dagger \times \exp\left\{\int_0^{1/T} d\tau\int d^2x\psi^\dagger(\tau,x)\left[-\frac{\partial}{\partial\tau} - H\right]\psi(\tau,x)\right\}, \quad (5)$$

where T is the temperature (the Boltzmann constant k_B is set equal to 1) and fermion fields ψ carry layer and spin indices.

The integration over the fermionic fields ψ takes into account low-energy electrons close to the charge neutrality point. Here the Hamiltonian $H = H_0 + V$ consists of two parts, the kinetic part of the free quasiparticles, H_0, in the underlying material and the interaction part, V, which describes the coupling between magnetic impurities and the itinerant electrons of twisted bilayer graphene [18,21–24]:

$$V = -\lambda[\mathbf{S}_1\cdot\mathbf{s}\delta(\mathbf{r}-\mathbf{R}_1)P_{l1} + \mathbf{S}_2\cdot\mathbf{s}\delta(\mathbf{r}-\mathbf{R}_2)P_{l2}]. \quad (6)$$

In this model spins $\mathbf{S}_1$ and $\mathbf{S}_2$ of two impurities are assumed to be classical, the $\boldsymbol{s} = \boldsymbol{\sigma}/2$ operator stands for the electron

spin in graphene expressed through the Pauli matrices, $\boldsymbol{R}_{1,2}$ are impurity positions, and P_{l1} and P_{l2} are the projectors onto the layers where the respective impurities are placed (layer indices $l1$ and $l2$ take the values of 1 and 2). These projectors are diagonal matrices $P_1 = \mathrm{diag}(1, 0)$ and $P_2 = \mathrm{diag}(0, 1)$. The coupling constant λ depends on the type of impurity placed on the graphene sheet. In what follows we consider Co impurities bound to carbon atoms in monolayer graphene, in this case the coupling reaches the value 1 eV a_C, where a_C is the area per carbon atom, $\simeq 2.62\text{Å}^2$ [25].

Since the action in the partition function is quadratic in fermionic fields, we find the following result for the free energy:

$$F = -T \ln \frac{\mathrm{Det}\left[-\frac{\partial}{\partial\tau} - H\right]}{\mathrm{Det}\left[-\frac{\partial}{\partial\tau} - H_0\right]} = -T\,\mathrm{Tr}\ln\left(\left[-\frac{\partial}{\partial\tau} - H\right]\left[-\frac{\partial}{\partial\tau} - H_0\right]^{-1}\right). \quad (7)$$

Here the Tr operation includes matrix trace tr, summation over valleys, and integration over coordinates. The last expression can be rewritten in terms of the free particle Green's function via the substitution $-\frac{\partial}{\partial\tau} - H_0 = G_0^{-1}$. This leads to the corresponding series expansion in powers of the coupling constant λ:

$$F = -T\,\mathrm{Tr}\ln(1 - V\hat{G}_0) = -T\,\mathrm{Tr}\left(-V\hat{G}_0 - \tfrac{1}{2}V\hat{G}_0V\hat{G}_0 - \tfrac{1}{3}V\hat{G}_0V\hat{G}_0V\hat{G}_0 - \tfrac{1}{4}V\hat{G}_0V\hat{G}_0V\hat{G}_0V\hat{G}_0 - \cdots\right). \quad (8)$$

In this expansion even powers of V terms contain contributions to the RKKY quadratic interaction, and starting at fourth order, additional biquadratic interactions appear (odd power terms vanish due to spin traces).

Now we analyze the second- and fourth-order contributions to the free energy. We evaluate the traces over spin matrix operators, taking into account that for graphene the Green's function is proportional to the unit matrix $\sigma_0 \equiv \hat{1}$ in real spin space. The combinatorial coefficients from spin traces δF_n^S enter the full nth-order correction to free energy as $\delta F = \lambda^n \delta F_n^S I_n$, and I_n contains integrals that depend on layer indices and distances between impurities. For the spin traces we find

$$\delta F_2^S = \tfrac{1}{4}\,\mathrm{tr}\,[S_{1,i}\sigma_i S_{2,j}\sigma_j] = \tfrac{1}{2}\boldsymbol{S}_1\boldsymbol{S}_2, \quad (9)$$

$$\delta F_3^S = \tfrac{1}{8}\,\mathrm{tr}\,[S_{1,i}\sigma_i S_{2,j}\sigma_j S_{1,k}\sigma_k] = \tfrac{1}{8}S_{1,i}S_{2,j}S_{1,k}\,\mathrm{tr}\,[\sigma_i(\delta_{jk} + i\varepsilon_{jkl}\sigma_l)] = 0, \quad (10)$$

$$\delta F_4^S = \tfrac{1}{16}\,\mathrm{tr}\,[(S_{1,i}\sigma_i)^4 + S_{1,i}\sigma_i S_{2,j}\sigma_j S_{1,k}\sigma_k S_{2,m}\sigma_m + \cdots] = \tfrac{1}{8}\left[\boldsymbol{S}_1^2 + \boldsymbol{S}_2^2 + 2\boldsymbol{S}_1\boldsymbol{S}_2\right]^2. \quad (11)$$

All odd contributions vanish due to the absence of odd power invariants composed of two spins that preserve rotational symmetry in space. In the next calculations we also do not take into account energy shifts appearing from terms not containing the dependence on the scalar product $\boldsymbol{S}_1\boldsymbol{S}_2$. Finally, from the expression for the fourth order, we extract constant terms and RKKY quadratic and biquadratic interactions:

$$\delta F_4^S = \tfrac{1}{8}\left[\left(\boldsymbol{S}_1^2 + \boldsymbol{S}_2^2\right)^2 + 4\left(\boldsymbol{S}_1^2 + \boldsymbol{S}_2^2\right)(\boldsymbol{S}_1\boldsymbol{S}_2) + 4(\boldsymbol{S}_1\boldsymbol{S}_2)^2\right]. \quad (12)$$

Having identified the orders and combinatorial coefficients of the leading contributions to the RKKY quadratic and biquadratic interactions, we proceed with the calculation of distance-dependent prefactors.

A. Expressions for distance-dependent prefactors

In this section we extract the distance-dependent prefactors in both the RKKY quadratic and biquadratic interaction terms and write them in terms of integrals over frequency. The corresponding interaction strengths, which depend on the distance R between two impurities, temperature, and chemical potential μ, are the prefactors of spin-dependent interaction terms:

$$\delta F = J_{\mathrm{quad}}(R, T, \mu)(\boldsymbol{S}_1\boldsymbol{S}_2) + J_{\mathrm{biq}}(R, T, \mu)(\boldsymbol{S}_1\boldsymbol{S}_2)^2. \quad (13)$$

Substituting the real space Green's function (4) into Eq. (8) and performing the summation over Matsubara frequencies by means of the well-known formula (B5), we arrive at the following expressions:

$$J_{\mathrm{quad}}(R, T, \mu) = \frac{\lambda^2}{16(\hbar v_F^*)^4} I^{(2)}_{l1,l2}(R, T, \mu) + \left(\boldsymbol{S}_1^2 + \boldsymbol{S}_2^2\right)\frac{\lambda^4}{64(\hbar v_F^*)^8} I^{(4)}_{l1,l2}(R, T, \mu), \quad (14)$$

$$J_{\mathrm{biq}}(R, T, \mu) = \frac{\lambda^4}{64(\hbar v_F^*)^8} I^{(4),\mathrm{biq}}_{l1,l2}(R, T, \mu). \quad (15)$$

Here the indices $l1$ and $l2$ denote the positions of impurities in the spinor components of the Hamiltonian (1) according to projectors (6). The summation over the valley index was already performed in these expressions and resulted in an additional factor of 2. In the lattice model the result can be further modified by the factor $1 + \cos(\Delta\boldsymbol{K}\boldsymbol{R})$, with $\Delta\boldsymbol{K} = \boldsymbol{K} - \boldsymbol{K}'$. In what follows, for numerical calculations we take cobalt atoms with effective spin $S = 3/2$ as impurities [26]. We recall that the spins of magnetic impurities are considered to be classical, so for cobalt $\boldsymbol{S}^2 = 9/4$.

The integrals defined above are expressed through Hankel functions. In the case of the quadratic RKKY interaction we have to evaluate the integrals:

$$I^{(m)}_{l1,l2}(R, \mu, T) = \int_{-\infty}^{\infty} \frac{d\omega f^{(m)}_{l1,l2}(\omega)}{e^{\frac{\omega-\mu}{T}} + 1}, \quad (16)$$

$$f^{(2)}_{l1,l2}(\omega) = \mathrm{Im}\left\{(\omega + i\varepsilon)^2\left[H_n^{(1)}\left(\frac{(\omega + i\varepsilon)R}{\hbar v_F^*}\right)\right]^2\right\}, \quad (17)$$

$$f^{(4)}_{l1,l2}(\omega) = \mathrm{Im}\left\{(\omega + i\varepsilon)^4\left[H_0^{(1)}\left(\frac{(\omega + i\varepsilon)R}{\hbar v_F^*}\right)\right]^2 \times \left[H_n^{(1)}\left(\frac{(\omega + i\varepsilon)R}{\hbar v_F^*}\right)\right]^2\right\}, \quad (18)$$

where $n = 1 - \delta_{l1,l2}$. Here μ is the chemical potential, and T is temperature, measured in units of the hopping parameter t of monolayer graphene. In the case of biquadratic interaction,

we find a different expression for the $f(\omega)$ function:

$$f^{\rm biq}_{l1,l2}(\omega) = {\rm Im}\left\{(\omega+i\varepsilon)^4\left[H^{(1)}_n\left(\frac{(\omega+i\varepsilon)R}{\hbar v^*_F}\right)\right]^4\right\},$$
$$n = 1-\delta_{l1,l2}. \tag{19}$$

One should note that the above expression is the same as Eq. (18) in the case of impurities being on the same layer and sublattice, $l1 = l2$.

Some integrals above, for example, $I^{(2)}_{l1,l2}(R,\mu,T)$, can be evaluated using Mellin-Barnes transformation, which reduces them to a sum over various Meijer G functions. This procedure was discussed in Ref. [18]. However, to describe qualitative behavior, the numerical evaluations at finite temperature are more appropriate. Thus, in the following sections we first analyze zero-temperature expressions and then discuss the effects of finite temperature found by numerical evaluations.

IV. ZERO-TEMPERATURE LIMIT

In the case of the RKKY quadratic interaction at zero temperature the integral $^{(2)}_{l1,l2}(R,\mu,0)$ has the following analytic form in terms of Meijer's G function:

$$I^{(2)}_{l1,l2}(R,\mu,T=0) = \left(\frac{\hbar v^*_F}{R}\right)^3\frac{1}{\sqrt{\pi}}G^{30}_{24}\left((k_FR)^2\middle|\begin{matrix}2,1\\0,\frac{3}{2},\frac{3}{2}+n,\frac{3}{2}-n\end{matrix}\right). \tag{20}$$

Here the Fermi wave vector k_F is defined as $k_F = \mu/\hbar v^*_F$. For zero chemical potential we have

$$G^{30}_{24}\left(0\middle|\begin{matrix}2,1\\0,\frac{3}{2},\frac{3}{2}+n,\frac{3}{2}-n\end{matrix}\right) = \frac{(4n^2-1)\sqrt{\pi}}{8}. \tag{21}$$

Hence,

$$I^{(2)}_{l1,l2}(R,0,T=0) = \left(\frac{\hbar v^*_F}{R}\right)^3\frac{4n^2-1}{8}. \tag{22}$$

To study the asymptotical behavior of our functions at large distances, $k_FR \gg 1$, it is convenient to single out in the corresponding zero-temperature integrals the parts that are independent of the chemical potential: $I(\mu) = I(0) + \int_0^\mu$. For the integrals depending on μ we use an asymptotical expansion of Hankel's function (see Ref. [27]):

$$H^{(1)}_\nu(z) \simeq \sqrt{\frac{2}{\pi z}}\,e^{i\phi}\sum_{k=0}^{\infty} i^k\frac{a_k(\nu)}{z^k}, \tag{23}$$

where

$$\phi = z - \frac{2\pi\nu+\pi}{4}, \qquad a_k(\nu) = \frac{\Gamma\left(\frac{1}{2}-\nu+k\right)\Gamma\left(\frac{1}{2}+\nu+k\right)}{\Gamma\left(\frac{1}{2}-\nu\right)\Gamma\left(\frac{1}{2}+\nu\right)(-2)^k k!}.$$

Thus, we find an asymptotical behavior of the oscillating part at $k_FR \gg 1$:

$$I^{(2)}_{l1,l2}(R,\mu,T=0) = \left(\frac{\hbar v^*_F}{R}\right)^3\frac{(-1)^{n+1}}{4\pi}[4k_FR\sin(2k_FR) + (4n^2+1)\cos(2k_FR)]. \tag{24}$$

The same asymptotical behavior follows, of course, from Eq. (20). A similar expression was obtained earlier in studies of monolayer graphene [23,28] and a pseudospin-1 system [18] in which the corresponding J integral described the second-order interaction of impurities on sublattices.

For the case of zero temperature in the fourth-order term, we find the polynomial pre-factor $(\frac{\hbar v_F}{R})^5$ for interaction integrals. Simple analytical expressions are obtained for zero chemical potential by replacing integration over the negative real axis with integration over the positive imaginary axis. Then, using the well-known formula relating the Hankel function of the imaginary argument to the modified Bessel function, we obtain

$$I^{(4),{\rm biq}}_{l1,l2}(R,0,T=0) = \left(\frac{2}{\pi}\right)^4\left(\frac{\hbar v^*_F}{R}\right)^5\int_0^\infty dz z^4K^4_n(z) = \left(\frac{2}{\pi}\right)^4\left(\frac{\hbar v^*_F}{R}\right)^5 \times\begin{cases}0.046, & n=0\ (l1=l2),\\ 0.561, & n=1\ (l1\neq l2).\end{cases} \tag{25}$$

$$I^{(4)}_{l1\neq l2}(R,0,T=0) = \left(\frac{2}{\pi}\right)^4\left(\frac{\hbar v^*_F}{R}\right)^5\int_0^\infty dz z^4K^2_0(z)K^2_1(z) = \left(\frac{2}{\pi}\right)^4\left(\frac{\hbar v^*_F}{R}\right)^5\times 0.132, \tag{26}$$

$$I^{(4),{\rm biq}}_{l1=l2}(R,0,T=0) = I^{(4)}_{l1=l2}(R,0,T=0). \tag{27}$$

For the asymptotic behavior $k_FR \gg 1$ we find

$$I^{(4)}_{l1,l2}(R,\mu,T=0) = \left(\frac{\hbar v^*_F}{R}\right)^5\frac{(-1)^{n+1}}{8\pi^2} \times[-8(k_FR)^2\cos(4k_FR) + 8n^2(k_FR)\sin(4k_FR) + (3-6n^2+4n^4)\cos(4k_FR)], \tag{28}$$

$$I^{(4),{\rm biq}}_{l1,l2}(R,\mu,T=0) = -\left(\frac{\hbar v^*_F}{R}\right)^5\frac{1}{8\pi^2}[-8(k_FR)^2\cos(4k_FR) + 16n^2(k_FR)\sin(4k_FR) + (3-12n^2+16n^4)\cos(4k_FR)]. \tag{29}$$

These results show that the biquadratic interaction $J_{\rm biq}$ generally has a much faster decay with distance than the quadratic one $J_{\rm quad}$. This is connected, of course, to the presence of a contribution of order λ^2 in the interaction strength $J_{\rm quad}$ [see Eqs. (14) and (15)]. Thus, the long-range ordered phases defined by biquadratic interaction will be less stable with respect to perturbations. In Fig. 2 we compare the results of numerical evaluation for two different distances between impurities and chemical potential $\mu = 1$ meV with respect to the change in

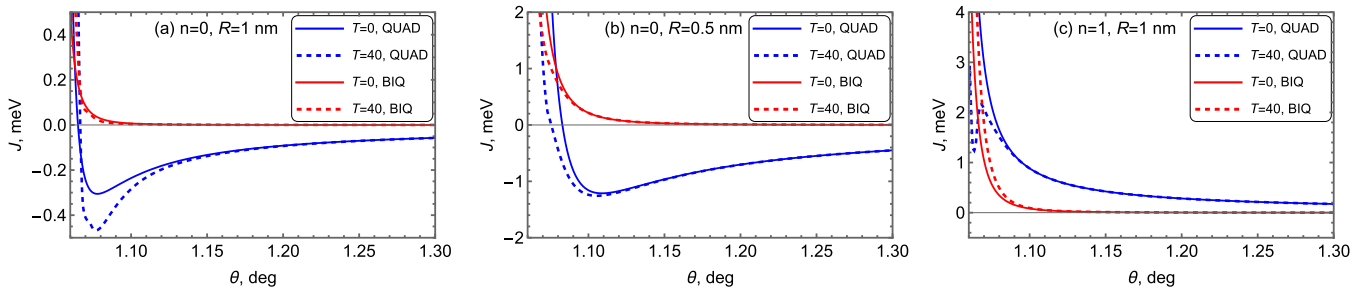

FIG. 2. Comparison of interaction strength dependences on the twist angle for $n = 0$ (same layer) and $n = 1$ (different layers). Interactions are evaluated via the integrals listed in Sec. IV for zero temperature $T = 0$, while the temperature corrections for $T = 40$ K are accounted with the integrals from Sec. V. The interaction constant $\lambda = 1\,\text{eV} \times 2.62\text{Å}^2$, and the distance between impurities $R = 1$ nm in (a) and (c), while $R = 0.5$ nm in (b). The chemical potential $\mu = 1$ meV lies within the applicability range of the low-energy model for almost all angles. The strong enhancement of both interactions happens close to the magic angle. For the $(n = 0)$-type interaction it is possible to find zero quadratic interaction while having a nonzero biquadratic one.

twist angle value. Let us emphasize that the $J > 0$ coupling for quadratic interaction is of the ferromagnetic type, while $J < 0$ is antiferromagnetic.

As is known for monolayer and bilayer graphene, the spin-spin interactions are generally weak. But in the vicinity of the magic angle, where the Dirac dispersion has a low effective Fermi velocity, interactions are strongly enhanced. That is clearly visible in all panels of Fig. 2. In addition, the oscillatory structure of the interactions starts playing a role. The mathematical origin of these oscillations is related to the quickly growing argument of Hankel functions under integrals when v_F^* goes to zero. The growth of $1/v_F^*$ also sets a limit on the applicability of perturbative expansion in Eq. (14). The dimensionless factor of the form $\lambda^2/(2\hbar v_F^* R)^2$ controls the ratio between the first and second terms and reaches a value of 1 for angle $\theta = 1.08^\circ$ and distance between impurities $R = 1$ nm (see Appendix C). At the same time, the small values of the integrals in Eqs. (25) and (26) further extend the applicability range, which is applied in Fig. 2. Figures 2(a) and 2(b) show a sequence of points at which the RKKY quadratic interaction passes zero while the biquadratic one does not. This allows for turning off the RKKY quadratic interaction for twist angles below 1.1° and short distances. This feature can be used to obtain novel types of correlated states in twisted bilayer graphene by fine-tuning the distance between impurities. The dependence on chemical potential is weak in the applicability range of the model (see Appendix A). At the same time, the distance between impurities allows for efficient control of the relative strength between interactions.

In addition, we present an analysis of the distance dependence of the quadratic and biquadratic interactions in Fig. 3. Figure 3 shows the optimal fine-tuned position of impurities to achieve the suppression of quadratic interaction for a fixed doping level of 1 meV. This dependence should be compared with the same dependence for monolayer graphene (see Fig. 4). The results for monolayer graphene are obtained by setting the effective Fermi velocity to be the same as the usual one, $v_F^* \to v_F$, in all expressions. The biquadratic interaction in the case of monolayer graphene is much weaker even for a very high doping level. Thus, we should point out that, while our approach works for every Dirac-type system, suitable observable results are expected to appear for a larger constant λ of spin-spin interaction between impurities and band electrons.

V. TEMPERATURE DEPENDENCE

In this section we present the numerical results for the temperature-dependent case. The analysis contains both the twist angle dependence to estimate the possibility of observing the effect at high temperatures and the chemical potential dependence at specific values of the twist angle.

Numerical integration is performed by dividing the integration interval into two parts, $[-\infty, 0]$ and $[0, \infty]$, and changing

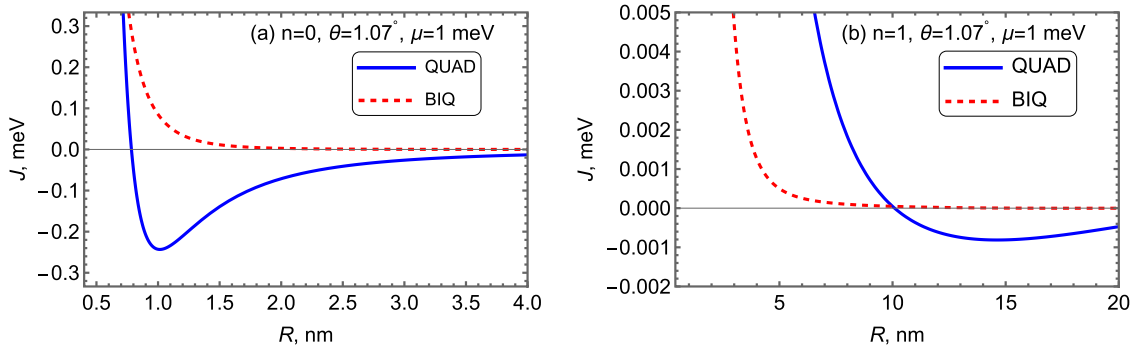

FIG. 3. Distance dependence of interactions for the zero-temperature case and a small chemical potential for the two example twist angles. The values of both interactions quickly decay with distance but have a larger relative value for the biquadratic interaction than in monolayer graphene (see Fig. 4).

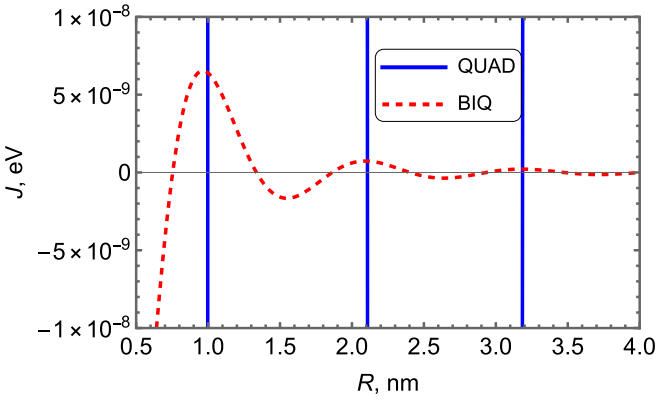

FIG. 4. Distance dependence of interactions for monolayer graphene at chemical potential $\mu = 0.9\,\text{eV}$ and the same sublattice position of impurities, $n = 0$. For the fine-tuned distance of impurities it is possible to achieve a dominant role of biquadratic interaction. However, the absolute values of both interactions for distances of impurities greater than 1 nm are small. Even for quadratic interaction, the interaction values are of the order of tens of meV [22,23].

the sign of ω in the first case. Replacing the variables in Eq. (16) with dimensionless ones, we find

$$I^{(m)}_{l1,l2}(R,T,\mu) = \left(\frac{\hbar v_F^*}{R}\right)^{m+1} \int_0^\infty dx f^{(m)}_{l1,l2}(x) \times \left(\frac{1}{ze^{x/T^*}+1} + \frac{z}{e^{x/T^*}+z} - 1\right), \quad (30)$$

where $T^* = \frac{TR}{\hbar v_F^*}$, $z = e^{-\mu/T}$. The last term in Eq. (30) (-1 in the parentheses) describes the contribution at zero temperature and $\mu = 0$; it diverges at the upper limit and thus requires a regularization. The appearance of divergences in separate terms of the perturbation series for the RKKY interaction was noticed long ago [29,30] and is related to the local nature of the RKKY interaction used. The regularization can be done either by replacing the polynomial part of the $f^m_{l1,l2}$ functions by $x^{\alpha-1}$ and further analytic continuation to the needed values of α (see, for example, [18]) or by implementing a finite frequency cutoff in the integral according to the energy range of applicability of the model (1). In the last case it is important to use smooth cutoffs instead of a sharp one to obtain cutoff-independent results in the long-distance limit [21]. There is also the issue of the convergence of the entire perturbation series for the RKKY interaction raised in the recent work of Rusin and Zawadzki [31], which we discuss in more detail in Sec. VI.

Taking into account the convergence subtlety in the expression above, the fully numerical calculation is more efficiently performed via the following equivalent partition into temperature-dependent and -independent parts:

$$I^{(m)}_{l1,l2}(R,T,\mu) = \left(\frac{\hbar v_F^*}{R}\right)^{m+1} \left[\int_{-\infty}^{k_F R} dx f^{(m)}_{l1,l2}(x) + T^* \int_0^\infty \times \frac{dx\left[f^m_{l1,l2}(k_F R + T^* x) - f^m_{l1,l2}(k_F R - T^* x)\right]}{e^x + 1}\right]. \quad (31)$$

In this form, the first term is known from Sec. IV. The last two terms represent a finite-temperature correction. In the brackets of the second integral, the function $f(\mu - Tx)$ might contain a jump at the point $x = \mu/T$. This feature is still integrable due to polynomial factors in all $f^n_{l1,l2}$ functions. However, it requires splitting of the integration interval at this point to ensure proper numerical convergence.

Performing the evaluation for different angles starting from close to the magic value $\theta = 1.05^\circ$, we find the results presented in Fig. 2. A comparison with the zero-temperature case shows that $T = 40\,\text{K}$ contributes a correction in Eq. (31) of the order of a few percent for most of the twist angle values. But it shifts the position of zero in quadratic interaction towards smaller angles. The structure of oscillations close to the first magic angle is altered; however, the zeros of quadratic interaction do not match the zeros of biquadratic interaction. Thus, it is still possible to fine-tune the system to a regime in which biquadratic interaction dominates. The varying value of the chemical potential has little influence on the results. The main contribution comes from the zero-doping integrals. Thus, we do not present a separate plot of the dependence on μ.

VI. CONCLUSIONS

In the present paper we studied the twist angle dependence of the RKKY quadratic and biquadratic spin-spin interactions between two magnetic impurities mediated by itinerant electrons in twisted bilayer graphene away from the magic angle. General expressions for both interactions were derived from the free energy of the system with two impurities. The qualitative analysis showed that quadratic and biquadratic interactions have different oscillating terms, and thus, regions in the parameter space of the angle, distance between impurities, chemical potential, and temperature where the biquadratic interaction dominates should exist.

Using analytic and numerical approaches, we showed that in all cases it is possible to identify the angle and distance for which the RKKY quadratic interaction vanishes while the biquadratic one remains finite. The dominant value of biquadratic interaction comparing to RKKY quadratic term can lead to the formation of the new correlated phases discussed in Refs. [7–10] when a number of impurities are sparsely placed on top of a graphene sheet. The oscillatory behavior of interactions close to the magic angle shows the effect of band flattening on the enhancement of both interactions with more fine-tuned competition between them.

Analyzing the results for an angle approaching the magic angle, we found the quick divergence of all interactions. From a mathematical point of view, this is a result of the trivial fact that the series expansion in $\lambda/\hbar v_F^* R$ loses its applicability due to vanishing Fermi velocity. The physics behind this is the divergent density of states when the system approaches the flat band. In this regard, a more thorough study should be carried out along the lines of that in Refs. [18,32] for the BM model.

Finally, we address the problem of convergence of the entire RKKY perturbation series raised in the very interesting recent work of Rusin and Zawadzki [31]. These authors obtained an exact RKKY Green's function for electrons with parabolic isotropic dispersion at zero temperature in

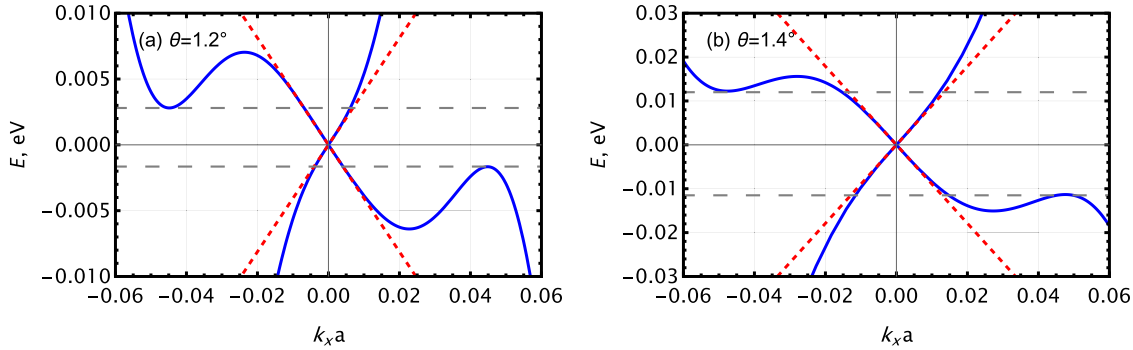

FIG. 5. Comparison of the effective Dirac model (1) (red dashed lines) and Bistritzer-MacDonald model spectrum (solid lines) with the band-touching point shifted to zero. Long-dashed lines show the chemical potential levels at which the linear Dirac model loses applicability independently of series expansion accuracy. This happens at local band minima, which are located slightly away from K points. Two different twist angles are shown.

three space dimensions. They got a criterion for the series convergence: the quantity $g_0 = G_{\text{free}}(r = 0, r' = 0)$ must be finite, where $G_{\text{free}}(r, r')$ is the free electron Green's function. Obtaining an exact Green's function in the considered model with the effective Hamiltonian (1) is an unsolved problem. Assuming that the convergence criterion will be similar, we see that in our case it is not fulfilled due to the integration by momenta of the free Green's function (3) up to infinity (g_0 is logarithmically divergent). Certainly, there is a natural cutoff k_c of the wave vector in the model under consideration, related to the applicability domain of the model (see Appendix A). Because of this, g_0 is finite, and one can expect the RKKY series of perturbation theory to converge.

The study of the RKKY interaction in this work indicates the ever-increasing role of such a control parameter as a twist angle in multilayer systems. For future study, we expect the numerical analysis of the full Bistritzer-MacDonald model and similar effective models for transition-metal dichalcogenides to be of great interest.

ACKNOWLEDGMENTS

D.O.O. acknowledges support from the Kavli Foundation. The work of T.T.O. and R.A.D. was supported by the Dutch Research Council (NWO) by the research program Fluid Spintronics under Project No. 182.069 and by OCENW.XL21.XL21.058. The work of V.P.G. was supported by the Swiss NSF within the Ukrainian-Swiss Joint research project "Transport and thermodynamic phenomena in low-dimensional materials with flat bands" (Grant No. IZURZ2_224624).

DATA AVAILABILITY

The data that support the findings of this article are openly available [33].

APPENDIX A: APPLICABILITY RANGE OF THE LINEARIZED MODEL

In this Appendix we discuss the applicability range of the linearized version of the BM model: the effective Dirac model near the band-touching point.

The main results are presented in Fig. 5. They show that the calculations within the Dirac model are limited to the narrow interval of chemical potentials. This interval is not symmetric on the positive and negative sides and shrinks towards zero when the twist angle approaches the magic value. In Figs. 5(a) and 5(b), we show that the intervals are $\mu \in [-1.65, 2.8]$ meV for $\theta = 1.2^\circ$ and $\mu \in [-11.5, 12]$ meV for $\theta = 1.4^\circ$. This limitation in energy of the linearized model naturally transforms into limiting the allowed values of the wave number to $k_c a \approx 0.01$.

APPENDIX B: EXACT EVALUATION OF THE SECOND -ORDER CONTRIBUTION TO FREE ENERGY

In this Appendix we demonstrate as an example of the calculations the second-order contribution of perturbation theory to the free energy defining the strength of the RKKY quadratic interaction. This contribution is given by the expression

$$\delta F_2 = \frac{\lambda^2 T}{2}\,\mathrm{tr}\int d\mathbf{r}_1 d\mathbf{r}_2 \int d\tau_1 d\tau_2 \Big\{\Big[\mathbf{S}_1\cdot\frac{1}{2}\boldsymbol{\sigma}\delta(\mathbf{r}_1-\mathbf{R}_1)P_{l1}+\mathbf{S}_2\cdot\frac{1}{2}\boldsymbol{\sigma}\delta(\mathbf{r}_1-\mathbf{R}_2)P_{l2}\Big]\sigma_0 G_0(\mathbf{r}_1,\mathbf{r}_2;\tau_1-\tau_2)$$
$$\times\Big[\mathbf{S}_1\cdot\frac{1}{2}\boldsymbol{\sigma}\delta(\mathbf{r}_2-\mathbf{R}_1)P_{l1}+\mathbf{S}_2\cdot\frac{1}{2}\boldsymbol{\sigma}\delta(\mathbf{r}_2-\mathbf{R}_2)P_{l2}\Big]\sigma_0 G_0(\mathbf{r}_2,\mathbf{r}_1;\tau_2-\tau_1)\Big\}. \tag{B1}$$

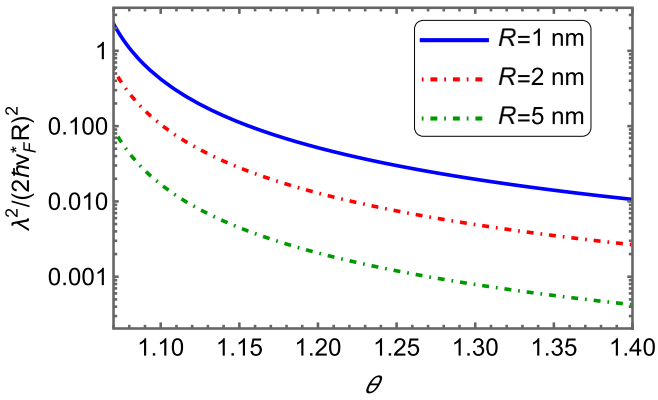

FIG. 6. The angle dependence of the dimensionless coupling constant that controls the ratio between RKKY and biquadratic interactions.

Evaluating the integrals over δ functions and performing the trace operation over the spin matrices, we find

$$\delta F_2 = \frac{\lambda^2}{4}\mathbf{S}_1\mathbf{S}_2 \int_0^{1/T} d\tau \,\mathrm{tr}[P_{l1}G_0(\mathbf{R}_1,\mathbf{R}_2;\tau)P_{l2}G_0(\mathbf{R}_2,\mathbf{R}_1;-\tau) + (l1\leftrightarrow l2,\mathbf{R}_1\leftrightarrow\mathbf{R}_2)]. \tag{B2}$$

The integration over τ can be equivalently rewritten as a sum over Matsubara frequencies using the Fourier transform of the imaginary-time Green's function,

$$G_0(\tau) = T\sum_{n=-\infty}^{\infty} G_0(i\omega_n)e^{-i\omega_n\tau}, \quad \omega_n = (2n+1)\pi T, \tag{B3}$$

where n is an integer. For δF_2 we get

$$\delta F_2 = \frac{\lambda^2}{2}\boldsymbol{S}_1\boldsymbol{S}_2 T\sum_n \mathrm{tr}\,[P_{l1}G_0(\boldsymbol{R};i\omega_n+\mu)P_{l2} \times G_0(-\boldsymbol{R};i\omega_n+\mu)], \tag{B4}$$

where $\boldsymbol{R} = \boldsymbol{R}_1 - \boldsymbol{R}_2$ and we introduced the chemical potential μ. The sum over the Matsubara frequencies is performed by means of the formula

$$T\sum_n f(i\omega_n) = -\int_{-\infty}^{\infty}\frac{d\omega}{\pi}n_F(\omega)\mathrm{Im}f^R(\omega+i\varepsilon), \tag{B5}$$

where $n_F(\omega) = 1/[\exp(\omega/T)+1]$ is the Fermi distribution function and the superscript R denotes the retarded function.

To obtain the results in the main text, one has to substitute the Green's function from Eq. (4) with ω replaced by $\omega+\mu$. In the considered case, the evaluation of the traces over sublattice-layer degree of freedom results in the function presented in Eq. (17). For example, for impurities placed on the same layer, we find

$$\mathrm{tr}\left[\begin{pmatrix}1&0\\0&0\end{pmatrix}\frac{\omega+\mu}{4(\hbar v_F)^2}\begin{pmatrix}-iH_0^{(1)}(z) & \xi e^{-i\xi\varphi}H_1^{(1)}(z)\\ \xi e^{i\xi\varphi}H_1^{(1)}(z) & -iH_0^{(1)}(z)\end{pmatrix} \times\begin{pmatrix}1&0\\0&0\end{pmatrix}\frac{\omega+\mu}{4(\hbar v_F)^2} \times\begin{pmatrix}-iH_0^{(1)}(z) & \xi e^{-i\xi(\pi+\varphi)}H_1^{(1)}(z)\\ \xi e^{i\xi(\pi+\varphi)}H_1^{(1)}(z) & -iH_0^{(1)}(z)\end{pmatrix}\right] = \frac{(\omega+\mu)^2}{16(\hbar v_F)^4}[H_0^1(z)]^2, \quad z = \frac{|\boldsymbol{R}|(\omega+\mu)}{\hbar v_F^*}. \tag{B6}$$

Similarly, we can evaluate the fourth-order correction to the free energy and thus arrive at the main expressions in Sec. III A.

APPENDIX C: THE CONVERGENCE OF SERIES EXPANSION

In this Appendix we analyze the convergence of series expansion by evaluating the relative coupling constant. This relative constant is defined as $\lambda^2/(2\hbar v_F^* R)^2$ and fixes the factor by which the terms following biquadratic interaction are suppressed. At the same time, it does not take into account the values of the zero-doping integrals, which could be smaller than 1. The dependence of dimensionless constant that controls convergence of series on twist angle is plotted in Fig. 6 for few different R values.

[1] W. Heisenberg, Zur theorie des ferromagnetismus, Z. Phys. **49**, 619 (1928).

[2] M. A. Ruderman and C. Kittel, Indirect exchange coupling of nuclear magnetic moments by conduction electrons, Phys. Rev. **96**, 99 (1954).

[3] T. Kasuya, A theory of metallic ferro- and antiferromagnetism on Zener's model, Prog. Theor. Phys. **16**, 45 (1956).

[4] K. Yosida, Magnetic properties of Cu-Mn alloys, Phys. Rev. **106**, 893 (1957).

[5] A. Kartsev, M. Augustin, R. F. L. Evans, K. S. Novoselov, and E. J. G. Santos, Biquadratic exchange interactions in two-dimensional magnets, npj Comput. Mater. **6**, 150 (2020).

[6] J. Y. Ni, X. Y. Li, D. Amoroso, X. He, J. S. Feng, E. J. Kan, S. Picozzi, and H. J. Xiang, Giant biquadratic exchange in 2D magnets and its role in stabilizing ferromagnetism of $NiCl_2$ monolayers, Phys. Rev. Lett. **127**, 247204 (2021).

[7] L. S. Lima, Quantum correlation in the bilinear–biquadratic model for iron-based superconductors, Eur. Phys. J. Plus **136**, 789 (2021).

[8] E. E. Kokorina and M. V. Medvedev, Magnetocaloric effect in a first-order phase transition in a ferromagnet with biquadratic exchange, Phys. Met. Metallogr. **122**, 1045 (2021).

[9] E. E. Kokorina and M. V. Medvedev, Quadrupole ordering and inverse magnetocaloric effect in a magnet with biquadratic exchange and spin S = 1, Phys. Met. Metallogr. **123**, 878 (2022).

[10] A. Szasz, C. Wang, and Y.-C. He, Phase diagram of a bilinear-biquadratic spin-1 model on the triangular lattice from density matrix renormalization group simulations, Phys. Rev. B **106**, 115103 (2022).

[11] R. Bistritzer and A. H. MacDonald, Moiré bands in twisted double-layer graphene, Proc. Natl. Acad. Sci. USA **108**, 12233 (2011).

[12] J. M. B. Lopes dos Santos, N. M. R. Peres, and A. H. Castro Neto, Graphene bilayer with a twist: Electronic structure, Phys. Rev. Lett. **99**, 256802 (2007).

[13] G. Li, A. Luican, J. M. B. Lopes dos Santos, A. H. Castro Neto, A. Reina, J. Kong, and E. Y. Andrei, Observation of Van Hove singularities in twisted graphene layers, Nat. Phys. **6**, 109 (2010).

[14] Y. Cao, V. Fatemi, S. Fang, K. Watanabe, T. Taniguchi, E. Kaxiras, and P. Jarillo-Herrero, Unconventional superconductivity in magic-angle graphene superlattices, Nature (London) **556**, 43 (2018).

[15] Y. Cao, V. Fatemi, A. Demir, S. Fang, S. L. Tomarken, J. Y. Luo, J. D. Sanchez-Yamagishi, K. Watanabe, T. Taniguchi, E. Kaxiras, R. C. Ashoori, and P. Jarillo-Herrero, Correlated insulator behaviour at half-filling in magic-angle graphene superlattices, Nature (London) **556**, 80 (2018).

[16] B. Lian, Z. Wang, and B. A. Bernevig, Twisted bilayer graphene: A phonon driven superconductor, Phys. Rev. Lett. **122**, 257002 (2019).

[17] G. Catarina, B. Amorim, E. V. Castro, J. M. V. P. Lopes, and N. M. R. Peres, Twisted bilayer graphene: Low-energy physics, electronic and optical properties, in *Handbook of Graphene*, Vol. 3, *Graphene-like 2D Materials*, edited by M. Zhang (Wiley, Hoboken, NJ, 2019), Chap. 6, p. 177.

[18] D. O. Oriekhov and V. P. Gusynin, RKKY interaction in a doped pseudospin-1 fermion system at finite temperature, Phys. Rev. B **101**, 235162 (2020).

[19] N. F. Q. Yuan, H. Isobe, and L. Fu, Magic of high-order van Hove singularity, Nat. Commun. **10**, 5769 (2019).

[20] A. S. Shankar, D. O. Oriekhov, A. K. Mitchell, and L. Fritz, Kondo effect in twisted bilayer graphene, Phys. Rev. B **107**, 245102 (2023).

[21] S. Saremi, RKKY in half-filled bipartite lattices: Graphene as an example, Phys. Rev. B **76**, 184430 (2007).

[22] M. Sherafati and S. Satpathy, RKKY interaction in graphene from the lattice Green's function, Phys. Rev. B **83**, 165425 (2011).

[23] M. Sherafati and S. Satpathy, Analytical expression for the RKKY interaction in doped graphene, Phys. Rev. B **84**, 125416 (2011).

[24] E. Kogan, RKKY interaction in graphene, Phys. Rev. B **84**, 115119 (2011).

[25] J. Cao, H. A. Fertig, and S. Zhang, RKKY interactions in graphene Landau levels, Phys. Rev. B **99**, 205430 (2019).

[26] L. Fritz and M. Vojta, The physics of Kondo impurities in graphene, Rep. Prog. Phys. **76**, 032501 (2013).

[27] NIST Digital Library of Mathematical Functions, edited by F. W. J. Olver, A. B. Olde Daalhuis, D. W. Lozier, B. I. Schneider, R. F. Boisvert, C. W. Clark, B. R. Miller, B. V. Saunders, H. S. Cohl, and M. A. McClain, Chap. 10.17, https://dlmf.nist.gov/.

[28] N. Klier, S. Shallcross, S. Sharma, and O. Pankratov, Ruderman-Kittel-Kasuya-Yosida interaction at finite temperature: Graphene and bilayer graphene, Phys. Rev. B **92**, 205414 (2015).

[29] G. Vertogen and W. J. Caspers, Contact part of the hyperfine interaction and the Ruderman-Kittel-Kasuya-Yosida approximation, Phys. Rev. Lett. **16**, 904 (1966).

[30] S. P. Bowen, Divergences and phonons in the indirect interaction, Phys. Rev. Lett. **20**, 726 (1968).

[31] T. M. Rusin and W. Zawadzki, Exact Green's function approach to RKKY interactions, Phys. Rev. B **101**, 205201 (2020).

[32] K. Laubscher, C. S. Weber, M. Hünenberger, H. Schoeller, D. M. Kennes, D. Loss, and J. Klinovaja, RKKY interaction in one-dimensional flat-band lattices, Phys. Rev. B **108**, 155429 (2023).

[33] D. O. Oriekhov, T. T. Osterholt, R. A. Duine, and V. P. Gusynin, Code for "RKKY quadratic and biquadratic spin-spin interactions in twisted bilayer graphene," Zenodo, https://doi.org/10.5281/zenodo.15591563.